Scientific Visualization, 2024, volume 16, number 5, pages 98 - 108, DOI: 10.26583/sv.16.5.07

Research into the Application of Additive Technologies in the Development of Tools for Microdeformation of Sheet Blanks Made from Non-Ferrous Metals and Alloys

M.A. Petrov[1,A], D.H. Tran[2,A]

Moscow Polytechnic University

[1] ORCID: 0000-0002-2324-5057, petrovma_mospolytech@mail.ru
[2] ORCID: 0009-0008-7152-6487, tranhung.bk56@gmail.com

Abstract

The paper shows the results of manufacturing of stamping tools for microforming operations. The tools and their main parts were obtained by different additive manufacturing technologies, from different materials (polymers and metals). A non-contact 3D scanning system was used to obtain metrological information on the accuracy of individual parts and assembly/subassembly. It was found that in order to match the dimensions of prototypes with the drawing dimensions and fall within the tolerance field, it is necessary to design the initial 3D model taking into account the peculiarities of 3D printing technology, mechanical processing, as well as the performance characteristics of the tool, which can be obtained from the results of wear tests.

Keywords: 3D-printing, FFF, SLM, LCD, microforming, copper M1, brass L63, aluminium alloys, surface wear.

1. Introduction

The idea of new applied, production technologies is changing as fundamental research develops. With the emergence of high-tech industries, such as the microelectronics industry, the manufacturing of microdetails and products has become an important part of manufacturing technologies. Maneuvering between the size of products and their required quantity, the total share of blanking production has not decreased. On the contrary, the mass production of microdetails forces to take a more careful approach to the development of production technology in order to avoid a large percentage of defects. Microdeformation or microstamping processes remain an understudied area. The main fundamental prerequisites for the development of microstamping technology were claimed by the Hall-Petch equation based on the dislocation theory, according to which with a decrease in grain size there is a significant increase in the strength characteristic of the product, according to equation (1), for a certain degree of deformation (ε), which leads to a decrease in plastic properties [1, 2]. In [3], the change in plastic properties of tape blanks, with thicknesses of 20, 50, 150 and 200 μm, described by flow curves (Fig. 1), is considered. It can be seen that at a certain value of the ratio of the blank thickness to the average grain size (t/d) the graphs cease to be equidistant to each other and their intersection is observed or their order is disturbed (rectangular areas with green dashed boarder line), which indicates a change in the plastic trend with changes in geometric sizes. Such kind of phenomena are called as “size effects”.

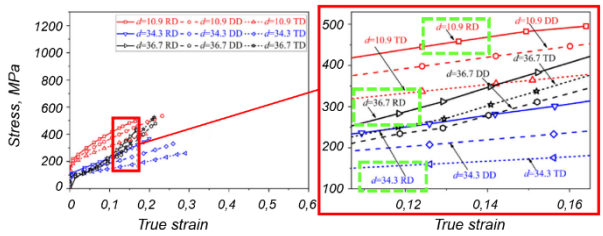

a) blank thickness 20 μm

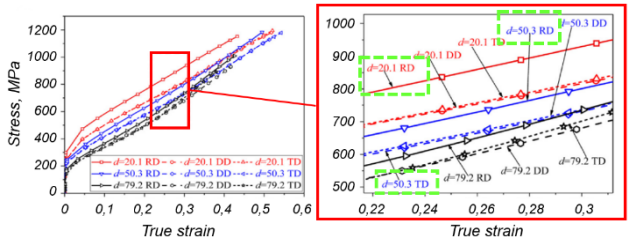

b) blank thickness 150 μm

Fig. 1. Flow stress curves for stainless steel SUS304 [3]

In other words, there is a minimum grain size, the fracture of which would require sufficiently high stresses. Accordingly, the plasticity of a metal sample is due to defects in the polycrystal, which is an aggregate of a large number of crystallites or grains of different sizes.

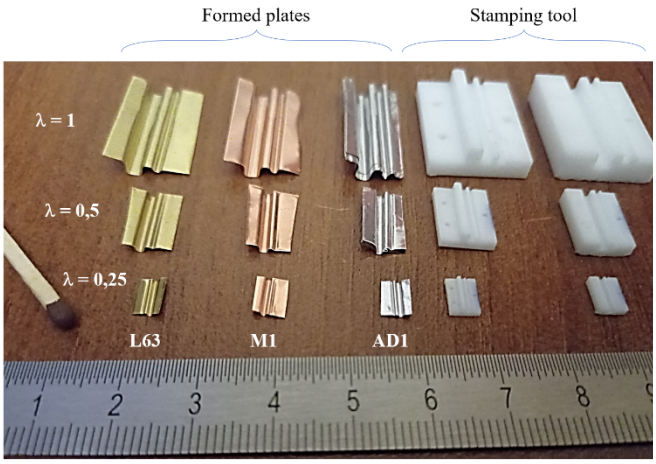

a) formed parts “Plate” and tools (common view)

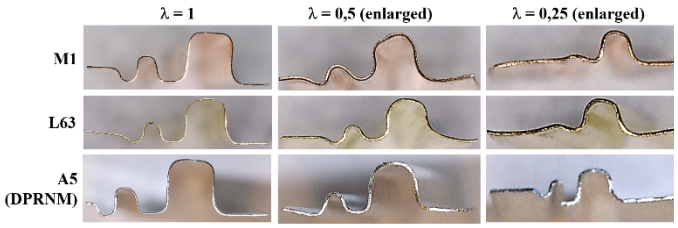

b) formed plates (side view)

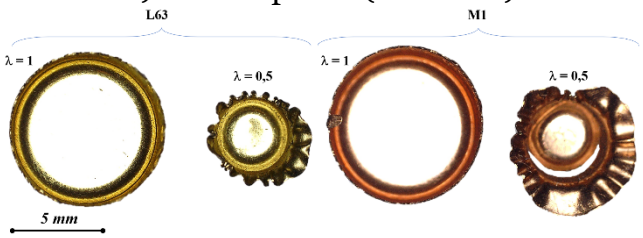

c) parts «Cup»

Fig. 2. Examples of formed microparts: flat (a, b) and axisymmetric (c) parts

Since the sizes of grains can vary in the range of macro- (up to 1 mm), micro- (from 1 mm to 1 μm) and nano-scales (from 1 μm to 1 nm), as well as have intermediate (meso-) levels, the question arises of studying the technological features of the deformation process at each of the levels. The dimensions of products, which can be contrasted with the grain size, can also be correlated to one of the mentioned dimensional levels. Usually, the transition from the micro to the macro level is characterized by the ability of an observer to view the product without a microscope. Our eye is able to see a detail the size of a speck of dust, but its shape or morphology is difficult to recognize without a microscope.

In this regard, separate scientific directions for studying materials and technologies at different dimensional levels are emerging. For micro-level products in English-speaking space there are such terms as microforming, microstamping, miniaturized and others [4-6].

The complexity of manufacturing of small-sized products lies in the need for additional means of objective process control and manipulation or positioning (placement in the working area, removal from the die and transfer to another position or container), as well as spe-

cialized equipment. The parts produced by microdeformation can be either sheet or bulk [7]. Fig. 2 shows the parts obtained by the authors of the article: samples of formed plates and cups obtained from different materials with different scaling factor (similarity) of the original geometry (λ). Sheet blanks, 0,1 mm thick, made of copper M1, brass L63 and and aluminium A5 (DPRNM), according to GOST 618-2014, were used for the study. To study the effect of gaps, aluminium foil, according to TU 1811-005-53974937-2004 and GOST 745-2014, 11 and 25 microns thick, folded several times to obtain the required thickness of the billet, was used. It can be clearly seen that structural materials behave differently in the process of their deformation, depending on the similarity coefficient. The waves in the flange region indicate insufficient clamping force of the flange region of the workpiece during the deformation process (Fig. 2c).

$$\sigma_т = \sigma_0 + \frac{k}{\sqrt{d}} \quad (1)$$

where $\sigma_т$ – yield point, MPa; σ_0 – friction stress, which includes contributions from solutes and particles but not from dislocations (e.g., for copper σ_0 = 20...25 MPa, aluminium σ_0 = 20 MPa, titanium σ_0 = 80 MPa [8, 9]); k – strength coefficient of material constant (e.g., for copper k = 0,11...0,14 MPa×m^{0,5}, aluminium k = 0,04 MPa×m^{0,5}, titanium k = 0,4 MPa×m^{0,5} [8, 9]); d – average grain size or crystallite.

The realization of the microstamping process requires an initial workpiece of a given thickness and diameter, a deforming tool, and a set of process parameters that determine the boundary conditions, such as ambient temperature, friction coefficient on the contact surfaces, etc. The tool is an expensive component one in this chain.

The working part of the tool has a complex profile and not always its manufacture is economically feasible in the traditional way, machining (subtractive technologies). In addition, mechanical, laser or electrochemical micromachining technologies are very expensive and require specialized equipment. In the XXI century, thanks to the development of hardware and software, it has become possible to create prototypes of products layer by layer, which reduces material consumption and makes it possible to manufacture complex products.

These technologies, called additive technologies or 3D printing, work with both metallic and polymeric materials. Fig. 3 shows graphs showing the advantage of manufacturing complex prototypes using additive manufacturing (AT) methods versus subtractive manufacturing (TT) methods. The resulting prototypes are necessarily post-processed, to a greater or lesser extent. It is this fact that makes it possible to make a choice either in favor of traditional or additive technologies.

Along with the advantage of building a complex geometry of the prototype there is a disadvantage of additive technologies, which is that the prototype receives a textured surface, due to the different way of building the object, the strategy of layer-by-layer processing or application of material, which depends on both the 3D printing technology and the parameters of the program controlling the printing process, and does not allow to use the prototype immediately after printing, and requires some finishing operations or post-processing.

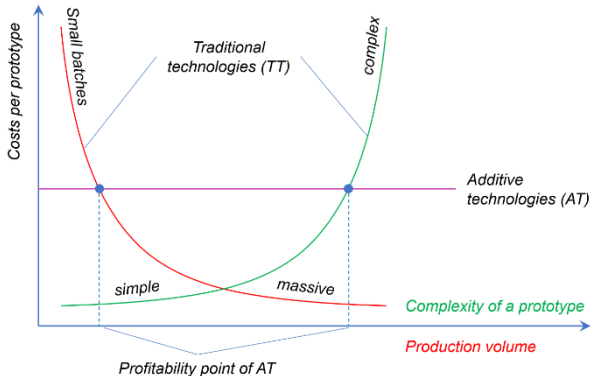

Fir. 3. Comparing plots for AT vs. TT

Texturing of the surface of a deforming tool can both improve and worsen the manufacturability of the microstamping process. For example, the surface microrelief affects the contact friction coefficient [10] and, consequently, the minimum and/or maximum microdrawing coefficient of the sheet blank, the blankholder force, and others. Also, depending on the 3D printing technology, there is a deviation of geometric dimensions from the dimensions of the original drawing [11].

Articles [12, 13] present the results of manufacturing the part "Cup" with the help of traditional tools, as well as tools that perform a combined operation of micro-cutting and microdrawing. A special tool was designed and manufactured using the SLM 3D printing technology with metal powder of heat-resistant steel with high cobalt content (Stellite 21), shown in Fig. 4. The part materials considered were 20...50 μm thick sheet blanks made of phosphor bronze, stainless steel, and titanium. The external diameter of the part "Cup" was ∅1,06 mm.

The obtained uniform fine-grained structure of Stellite 21 and the fine fraction of carbides made it possible to significantly increase tool life and obtain sheet microdetails without fracture. However, it should be noted that this was also facilitated by the proper choice of both the lubricant to reduce contact friction and the tool protective coating to reduce the intensity of surface wear.

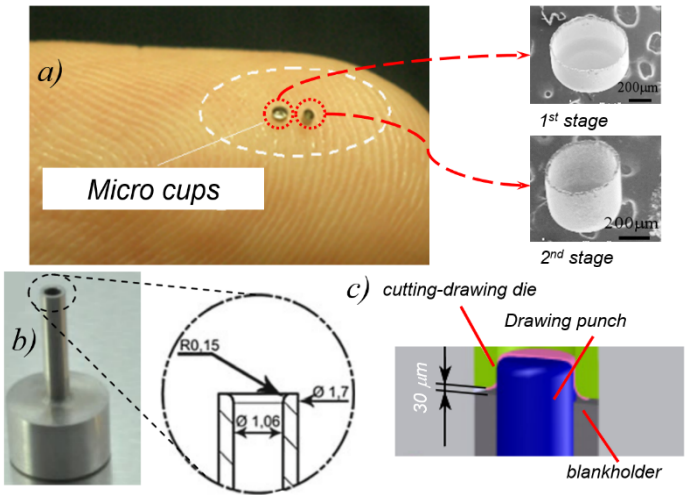

Fir. 4. Microparts (a) and stamping tool (b, c)

In [14], the technology of microprinting or SLμM (Selective Laser micro Melting) is used to obtain parts with a resolution of 50 μm and with high straight walls of the part at the micro level, in order to manufacture, for example, medical needles for drug transfer (Fig. 5a) or bifurcation stents (Fig. 5b) [15].

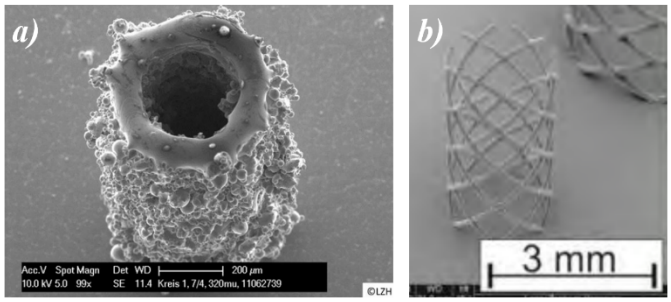

Fir. 5. Biomedical parts, manufactured using SLμM: needle (a) and stent (b)

2. Stamping tool's manufacturing

The microdrawing process was performed using a bottom-down drawing pattern, i.e., the part is oriented so that its bottom is at the bottom during microdrawing. Fig. 6 shows the variants of the deforming tool design.

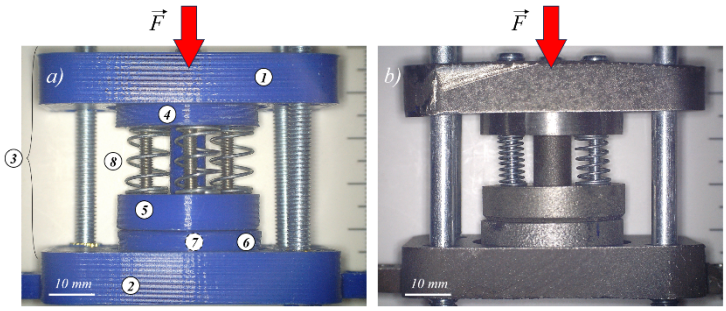

Fig. 6. Assembled stamping tool for microdrawing, made of: polymers (a) and metals (b).

The tool consists of upper (1) and lower (2) plates, guide sleeves and columns (3), punch with punch holder (4), blankholder (5), die holder (6) and die insert (7), located inside in the center of the die holder, as well as an elastic element in the form of compression springs (8).

Three 3D printing technologies were considered. DMLS and SLM technologies were used to fabricate the metal tool. FFF and LCD technologies were used to fabricate the polymer tool. A brief summary is presented in Table 1. Titanium alloy (VT6), stainless steels (03X17H12M2 and AISI316L) and aluminum alloy (AlSi10Mg) were considered as materials for metal 3D printing.

Polyethylene terephthalate-glycol (PETG) was used for manufacturing polymer prototypes of tool parts by extrusion printing method, and basic photopolymer (BPP) and ceramic-like photopolymer (CLPP) were used for mask photopolymer printing method. The study proceeded further according to the scheme presented in Fig. 7.

Table 1. Applied AT and materials

Technology	Company	Material
DMLS	3D Systems	VT6, AlSi10Mg (analog AK9)
SLM	3DLAM	03X17H12M2 (analog AISI 316L)
FFF	Anycubic	PETG
LCD	Creality-Halot	BPP, CLPP

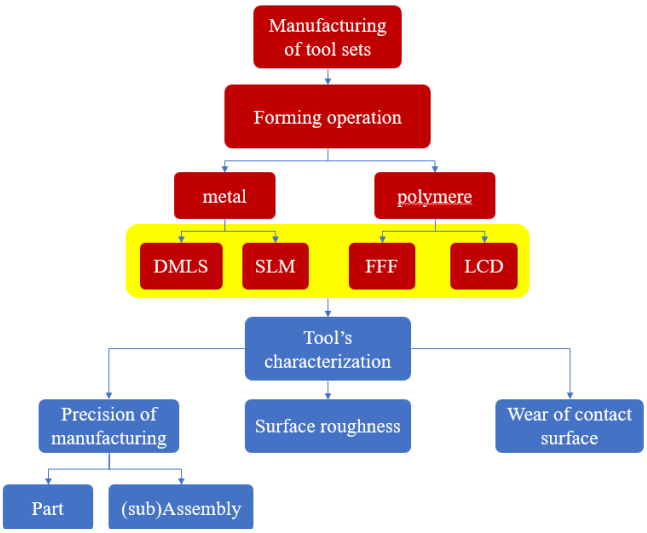

Fig. 7. Scheme of manufacturing and testing the stamping tools' parts

The FFF (Fused Filament Fabrication) extrusion-type 3D printing technology consists of layer-by-layer addition of polymer material fed from a spool of polymer wire ∅1,75 mm, passing through a hot zone and extruded through an extruder nozzle with a diameter of ∅0,4 mm, which is ~77% smaller than the original wire diameter. The prototype is grown in a bottom-up direction. Photopolymer 3D printing by mask technology (Liquid-Crystal Display) implies growing a prototype from a viscous photopolymer composition with UV curing, passing

through a liquid crystal matrix, on which cross-sections of the profile are generated, according to the control program of the 3D printer, works in the top-down direction. SLM (Selective Laser Melting) and DMLS (Direct Metal Laser Sintering) technologies allow to produce metal prototypes according to the bottom-up growth scheme by melting the material with the laser beam and its crystallization in cross-sections according to the control program (gcode).

The results of any 3D printing were followed by post-processing, including support removal, cleaning in isopropyl alcohol and water (LCD only), deburring and chamfering, threading and/or installation of threaded inserts and bushings, heat treatment (DMLS only), and more.

Figure 8 shows the results of 3D printing the punches. As the diameter of the punch increases, its surface appears smoother. Indeed, the reduction of the part size also affects the exposure time of the laser beam on the metal powder surface. With the same settings, the relative size (ratio of the max. melt bath size to the size of the section to be printed) and the rate (type) of melt bath crystallization will be different, resulting in different surface microrelief. However, by choosing the same printing settings for all punch sizes, as was the case in our case, a significant difference in microrelief was obtained. Performing also a comparison of the microrelief in one group of materials, stainless steel, (Figures 8g vs. 8d) it can be seen that the surface quality is quite different. This is due to a purposeful change in 3D printing technology on the same equipment.

BPP (Fig. 8e) and PETG (Fig. 8h) punches obtained by LCD and FFF techniques, respectively, have a pronounced layered microrelief due to printing accuracy and layer height.

3. Assessment of manufacturing precision

After 3D printing and post-processing of prototypes, the dimensions of individual parts as well as assembly units were controlled (Fig. 9). A non-contact 3D scanning method based on structured illumination was used to obtain information on product dimensions. Before scanning, all objects were coated with Ateco Ghost matting self-disappearing spray to obtain a uniform surface reflectance.

After receiving a series of scans by RangeVision Neopoint 3D scanner, their processing, final alignment and export of the polygonal (stl-) model of the actual object in RV 3D Studio program, the obtained result was compared with the original CAD-geometry in GOM Inspect program.

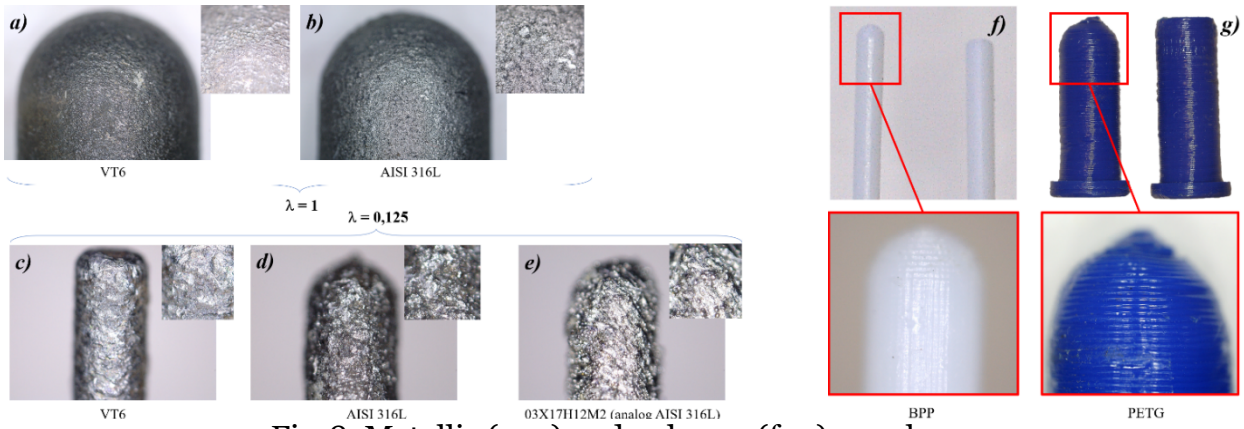

Fir. 8. Metallic (a–e) and polymer (f–g) punches

The accuracy of the final alignment for the die insert was 0,036 mm, and for the subassembly of the lower part of the tool was 0,085 mm. Alignment of the CAD model and the actual polygonal stl model was performed in two stages. In the first stage, alignment was performed either by a single point or by three matching points selected on each of the 3D models. In the second step, local best geometry matching was performed. The matching accuracy for the matrix in the first and second stages was 0,0524 mm. The matching accuracy for the subassembly in the first stage was 0,61 mm and in the second stage was 0,1618 mm.

The dimensions along the lateral outer surface of the die insert were found to lie outside the symmetrical tolerance of ±0,1 mm corresponding to 3D printing accuracy, resembling an ovality-type defect (Fig. 9a).

In the central part (die insert's hole and cylindrical wall), the red area indicates a high size mismatch, which is due to the lack of geometry information from the 3D scanning results. The subassembly of the lower part of the tool at the set symmetrical tolerance of ±1 mm is almost all within the tolerance field.

However, the histogram of the size distribution on the deviation map of geometric dimension (DMGD) plotted for the central section shows that the size difference between the original CAD model and the actual polygonal stl model is in the range of ±0,2, which is several times higher than the printing accuracy.

Based on the obtained results of the metrological evaluation, the inaccuracies at the 3D printing and assembly stages were determined. The obtained values of deviations indicate that it is possible to use printed tool parts without carrying out finishing operations of mating surfaces, but this requires taking into account the peculiarities of the 3D printing technology itself, surface microrelief, shrinkage and others. In this regard, the most rational approach would be to change the dimensions of the initial 3D model with consideration of the final machining.

a)

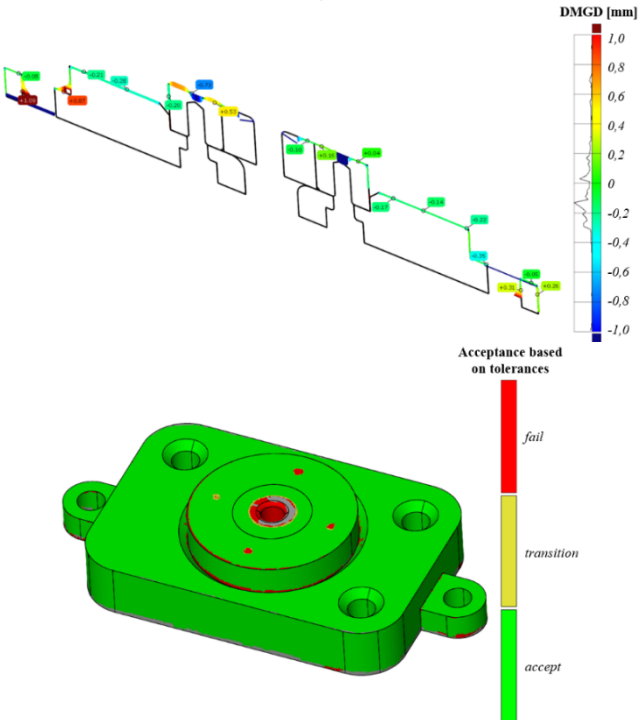

b)

Fig. 9. Dimension and tolerance visualization for printed tools' parts: die insert (a) and subassembly of the lower tools' part (b)

4. Characterizing the contact surface

Layer-by-layer principle of objects manufacturing leaves topography or microrelief highlighted the 3D printing method (Fig. 10).

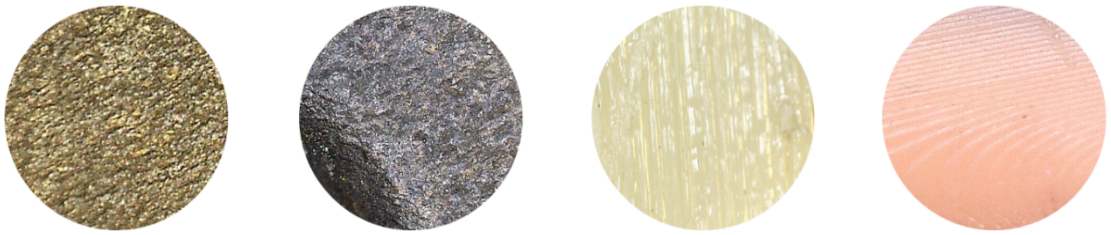

Fig. 10. Examples of surface topography of the tools' parts

Its description requires special tools that determine the surface roughness (GOST 2789-73, GOST R ISO 4287-2014). Thus, according to GOST R 70117-2022, in flat grinding, which is used as one of the final operations in the manufacture of deforming tools, the surface roughness varies in the range of Ra 6.3...0.05 microns. The roughness of the printed prototypes varies in a different range. This circumstance allows us to think that also technological parameters of the process of pressure processing will not correspond to those adopted in the development of traditional technologies, i.e. with the use of tools obtained by machining.

For roughness measurement a roughness meter TR210 (Time Group Inc., China) was used, at the measuring lengths of 0,25 and 0,8 mm, and a profilometer MarSurf M400 (Mahr GmbH, Germany), at the measuring length of 2,5 mm. Roughness was measured on the surfaces of prototypes of individual tool representative parts made of VT6, PETG, BPP and CLPP. According to the measurement device, the following roughness values presented in Table 2 were obtained. The surface wear was determined based on the results of experiments using the "pin-on-plate" technique on a CSM TRB tribometer (Fig. 11).

Table 2. Values of roughness measurements

Material	**Ra**		
	0,25	0,8	2,5
VT6	1,42	3,68	6,63
PETG	0,66	1,33	6,77
BPP	0,29	0,75	0,31
CLPP	1,10	1,27	0,64
Material	**Rz**		
VT6	7,56	20,26	22,18
PETG	3,06	6,43	22,73
BPP	1,44	4,55	1,63
CLPP	5,05	9,24	3,02

In the course of the experiment, the substrate (workpiece material) received translational reciprocating motion for a total path length equal to S=500 m. At the same time, a pin tip touched the substrate. The pin was loaded with normal force. The wearable pin tip had a hemispherical shape and was made of the same material as the tools' materials under study.

After passing the specified path, the substrate material and the rod tip were removed from the testing machine. Determination of the wear rate was carried out using Archard's equation (2), for which the amount of wear on the pin tip material was determined based on the known tip shape diameter and segment height after wear, equations (3) and (4), respectively. The determination of segment height can be done in several ways. First, after direct measurement of the wear scare using a microscope (digital or electronic), the segment height is determined using equation (4) (technique A). Secondly, it is possible to perform calculations in a CAD software, using geometric constructions, based on the known initial radius of the hemispherical pin tip and the wear scare diameter (method B).

Fig. 12 shows the wear of the hemispherical pin tip under electron (a) and digital (b) microscopes.

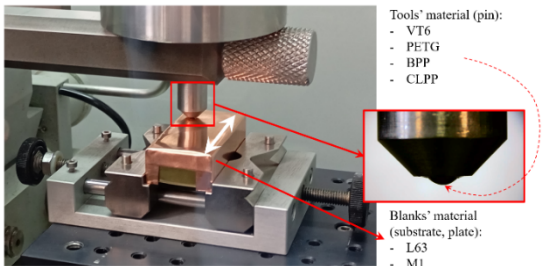

Fig. 11. Equipment for surface wear test based on scheme "pin-on-plate"

$$K = \frac{WH}{F_N S} \tag{2}$$

$$W = \frac{\pi h}{6}\left(\frac{3d_w^2}{4} - h^2\right) \tag{3}$$

$$h = R - \sqrt{\left(R^2 - \frac{d_w^2}{4}\right)} \tag{4}$$

where W – volume loss of the pin's tip, mm³; K – wear coefficient; F_N – normal reaction force, 1...5 N; S – distance length, mm; H – hardness of less harder material, N/mm²; h – height of the segment of weared material, мм; d_w – wear scare diameter, mm; R – initial radius of the hemi-spherical pin's tip, mm.

Note that the hemispherical tip has two wear areas. Thus, an additional wear area can be said to be formed due to the formation of a bump on the substrate. Ideally, the formation of a bump should be avoided, the appearance of which is associated with a high normal force (F_N) applied to the rod, indicating either a need to reduce the weight of the load or to reduce the length of the total sliding distance (S). The formation of the second region can also be attributed to CLPP pitting during the experiment.

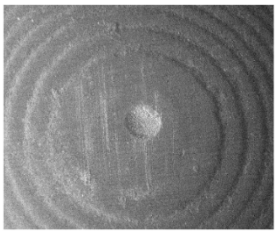

a)

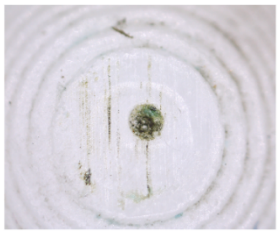

b)

Fig. 12. Visual control of the CLPP pin's tip wear under microscope: electronic (a) and digital (b)

5. Discussion of the results

Ыефьзштп tools obtained by 3D printing methods allow to produce miniature parts in the volume of a small batches (10...50 pieces). At the same time, the change in geometry occurs on the working parts of the tool, on the punch and die insert, which requires their remanufacturing.

The study of microrelief made it possible to evaluate the roughness of prototype parts of the stamping tool.

Using tribometer and microscopes, wear of the tools' materials was investigated for the fabrication of an axisymmetric part. Considering wear tests as a source of information about the wear coefficient under linear loading of the 3D printed tool material, it is possible to perform a preliminary assessment of the wear of the curvilinear surface of the die insert entry by any numerical method, for example, with the help of finite element simulation of the microdrawing process.

Elimination of manufacturing inaccuracies may lead to minimization of the advantages of additive manufacturing technologies compared to traditional technologies, so it is necessary to take into account in advance in the geometry of the digital model the machining tolerances.

6. Conclusions

Additive technologies are a promising way to manufacture a variety of tools with high accuracy and complexity. The tasks set for 3D printing of tools from metal and polymer materials for stamping sheet blanks can be accomplished, but need justification for estimating the manufacturing accuracy and performance characteristics that affect the accuracy and quality of the part, and tuning the technological parameters of the deformation process, respectively. Applying the known methods of surface microrelief and wear assessment for macro level it is also necessary to justify the extension of these results to the micro level, which requires practical confirmation on specialized equipment operating on micro-sized samples.

References

1. Hall, E. O. (1951). The Deformation and Ageing of Mild Steel: III Discussion of Results. Proceedings of the Physical Society. Section B, 64(9), 747–753. DOI:10.1088/0370-1301/64/9/303
2. Petch, N.J. The cleavage strength of polycrystals. J. Iron Steel Inst. 1953, 174, 25–28
3. B. Meng, W.H. Wang, Y.Y. Zhang, M. Wan, Size effect on plastic anisotropy in microscale deformation of metal foil, Journal of Materials Processing Technology, Vol. 271, 2019, Pages 46-61. DOI: 10.1016/j.jmatprotec.2019.03.023
4. Geiger, M., Kleiner, M., Eckstein, R., Tiesler, N., & Engel, U. (2001). Microforming. CIRP Annals, 50(2), 445–462. DOI:10.1016/s0007-8506(07)62991-6
5. Fu, M. W., & Chan, W. L. (2014). Micro-scaled Products Development via Microforming. Springer Series in Advanced Manufacturing. DOI:10.1007/978-1-4471-6326-8
6. Jiang Z., Zhao J., Xie H. Microforming Technology: Theory, Simulation, and Practice, Academic Press, 2017. — 458 p. — ISBN: 978-0-12-811212-0.
7. Xu, J., Wang, X., Wang, C., Yuan, L., Chen, W., Bao, J., Guo, B. (2020). A Review on Micro/Nanoforming to Fabricate 3D Metallic Structures. Advanced Materials, 33(6), 2000893. DOI:10.1002/adma.202000893
8. Hansen, N. (2004). Hall–Petch relation and boundary strengthening. Scripta Materialia, 51(8), 801–806. DOI:10.1016/j.scriptamat.2004.06.002
9. Smith W.F., Hashemi J. Foundations of Materials Science and Engineering, 7th Edition. — McGraw-Hill, 2023. — 1137 p. — ISBN 978-1260597709.
10. Wang, C., Guo, B., & Shan, D. (2014). Friction related size-effect in microforming – a review. Manufacturing Review, 1, 23. DOI:10.1051/mfreview/2014022
11. Kuhfuss, B. et al. (2020). Micro Forming Processes. In: Vollertsen, F., Friedrich, S., Kuhfuß, B., Maaß, P., Thomy, C., Zoch, HW. (eds) Cold Micro Metal Forming. Lecture Notes in Production Engineering. Springer, Cham. DOI: 10.1007/978-3-030-11280-6
12. Shimizu, T., Yang, M., & Manabe, K. (2012). Impact of Surface Topography of Tools and Materials in Micro-Sheet Metal Forming. Metal Forming - Process, Tools, Design. DOI:10.5772/48296
13. Kuhfuss, B. et al. (2020). Micro Forming Processes. In: Vollertsen, F., Friedrich, S., Kuhfuß, B., Maaß, P., Thomy, C., Zoch, HW. (eds) Cold Micro Metal Forming. Lecture Notes in Production Engineering. Springer, Cham. DOI: 10.1007/978-3-030-11280-6
14. Gieseke, M., Senz, V., Vehse, M., Fiedler, S., Irsig, R., Hustedt, M., … Haferkamp, H. (2012). Additive Manufacturing of Drug Delivery Systems. Biomedical Engineering / Biomedizinische Technik, 57(SI-1 Track-S). DOI:10.1515/bmt-2012-4109
15. Track F. (2014). Biomedical Engineering / Biomedizinische Technik, 59(Supplement). DOI:10.1515/bmt-2014-5005